ELSEVIER

Journal of Nuclear Materials 270 (1999) 279–289

journal of nuclear materials

Zr-rich layers electrodeposited onto stainless steel cladding during the electrorefining of EBR-II fuel

Dennis D. Keiser Jr. *, Robert D. Mariani

Argonne National Laboratory-West, P.O. Box 2528, Idaho Falls, ID 83403-2528, USA

Received 18 May 1998; accepted 8 December 1998

Abstract

Argonne National Laboratory is developing an electrometallurgical treatment for spent nuclear fuels. The initial demonstration of this process is being conducted on U–Zr alloy fuel elements irradiated in the Experimental Breeder Reactor II (EBR-II). We report the first metallographic characterization of cladding hull remains for the electrometallurgical treatment of spent metallic fuel. During the electrorefining process, Zr-rich layers, with some U, deposit on all exposed surfaces of irradiated cladding segments (hulls) that originally contained the fuel alloy that was being treated. In some cases, not only was residual Zr (and U) found inside the cladding hulls, but a Zr-rind was also observed near the interior cladding hull surface. The Zr-rind was originally formed during the fuel casting process on the fuel slug. The observation of Zr deposits on all exposed cladding surfaces is explained with thermodynamic principles, when two conditions are met. These conditions are partial oxidation of Zr and the presence of residual uranium in the hulls when the electrorefining experiment is terminated. Comparisons are made between the structure of the initial irradiated fuel before electrorefining and the morphology of the material remaining in the cladding hulls after electrorefining.

1. Introduction

Argonne National Laboratory (ANL) is developing an electrometallurgical treatment for spent nuclear fuels [1]. The demonstration of the process is being performed on irradiated U–Zr fuel elements from the Experimental Breeder Reactor II (EBR-II) located in Idaho. The electrometallurgical treatment process utilizes chopped fuel segments in perforated, steel, anode baskets as feedstock to an electrorefiner. The anode baskets are immersed in molten eutectic LiCl/KCl salt at 773 K. Current is applied to dissolve uranium, actinides, and fission products from the cladding segments, and the uranium is deposited on a steel mandrel that serves as a cathode. The cladding hulls, noble metal fission products, [1] and most of the zirconium, a constituent of the metallic fuel, are left behind in the anode basket. This material is run through a distillation furnace to remove adhering salt, and then it is consolidated into a metal waste form (MWF) ingot in an induction furnace [2,3]. The MWF is slated for eventual disposal in a geologic repository.

Detailed characterization of the material that remains in the anode baskets has been performed after different runs of the electrorefiner. Since this material comprises the majority of the MWF, it is important to characterize it. Additionally, the form and quantity of the material left behind in the cladding hulls is related to the specific operating conditions of the electrorefiner. Characterization of unirradiated and irradiated cladding hulls issuing directly from the electrorefiner has been completed using a scanning electron microscope (SEM) situated in a shielded glovebox. Chemical analysis has been performed on samples to assist in determining what is left behind with the cladding hulls after electrorefining. Since much analysis has been performed on fuel elements irradiated in EBR-II, it is possible to construct a before and after electrorefining scenario. In this

* Corresponding author. Tel.: +1-208 533 7298; fax: +1-208 533 7863; e-mail: dennis.keiser@anl.gov

[1] Noble metal fission products include Ru, Pd, Rh, Tc, etc. (see Table 1).

0022-3115/99/$ – see front matter
PII: S0022-3115(99)00011-2

context, the microstructures of the fuel and cladding in a representative fuel element irradiated in EBR-II will be described and then related to the material left behind with the cladding hulls after electrorefining. Finally, the thermodynamic driving forces which allow for deposition of Zr-rich layers on exposed surfaces of cladding hulls, under certain electrorefiner conditions, will be discussed.

2. Experimental procedure

The electrorefiner is a steel vessel 1.0 m deep and 1.0 m in diameter (Fig. 1). It is located in the Fuel Conditioning Facility argon hot cell. While most of the electrorefining experiments have been conducted at 773 K, some have been conducted at 723 K. The vessel is filled with molten cadmium to a nominal depth of 10.2 cm. On top of the molten cadmium rests the electrolyte, molten LiCl/KCl (41.0 mol% KCl) at the eutectic composition, to a nominal depth of 33.0 cm. UCl_3 is dissolved in the electrolyte with a nominal concentration of 9.0 wt.%. Four ports (25.0 cm diameter) on the cover of the electrorefiner are used to install anodes and cathodes into the electrorefiner.

2.1. Electrochemical dissolution of irradiated fuel

In the electrorefining process, uranium metal is oxidized to U^{3+} (UCl_3) at the anode, and U^{3+} is reduced to uranium metal at the cathode. The reactions are given by

$$\text{Anode Reaction}: \quad \text{U(feedstock)} \rightarrow U^{+3} + 3e-, \qquad (1)$$

$$\text{Cathode Reaction}: \quad U^{+3} + 3e- \rightarrow \text{U(electrorefined)}. \qquad (2)$$

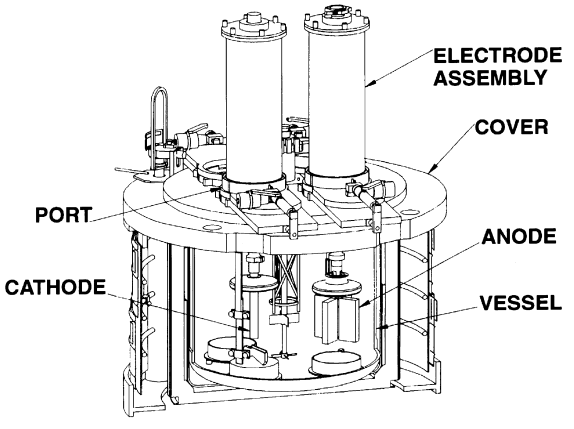

Fig. 1. Schematic diagram of the fuel conditioning facility electrorefiner.

The feedstock to the electrorefining process is spent fuel from EBR-II. Prior to entering the reactor, the fuel slugs are cast as a U–10Zr metal alloy, [2] less than 0.58 cm in diameter and approximately 34.3 cm long. In the fuel fabrication process, a fuel slug is loaded into a stainless steel cylinder cladding, approximately 0.58 cm in diameter and 74.9 cm long. The cladding wall thickness is 0.038 cm. The fuel element is welded to provide a hermetic seal. Prior to welding the fuel element, a small amount of sodium metal is added to provide a thermal bond between the fuel slug and the cladding (the sodium is liquid at the reactor's operating temperature). Upon removal from the reactor, the uranium content in the spent fuel is reduced by approximately 8.0%. A typical electrorefiner feedstock composition is given in Table 1 [4,5]. Some initial electrorefiner tests were run using unirradiated fuel elements and so the feedstock for these tests had the typical alloy composition of U–10Zr.

To make an anode assembly, the lower 38 to 41 cm of 122 spent fuel elements are mechanically chopped into 0.64 cm segments and loaded into four rectangular, perforated steel fuel dissolution baskets (FDBs). The remaining plenum portions of the fuel elements are set aside for the MWF. The four FDBs are assembled together in a '+' geometry to form an anode assembly. This assembly is then immersed (23 cm) into the molten salt electrolyte of the electrorefiner. The anode assembly is connected to the anode (positive) lead of a d.c. power supply that can operate either in controlled current or controlled voltage mode. During electrorefining, the anode assembly is rotated (speeds of 5, 25, and 75 rpm have been used). The electrorefiner operating conditions for the cladding hulls used in this study are given in Table 2.

For removing uranium from the electrorefiner, the cathode consists of a steel rod, 6.67 cm diameter, immersed in the electrolyte (23 cm). It is connected to the cathode (negative) lead of the power supply. Purified uranium dendrites grow on the steel cathode, which is rotated at 5 or 20 rpm. The size of the deposit is constrained radially to 25 cm by the action of a scraper, mounted on the inside electrorefiner wall, as the deposit rotates. The size of the deposit is constrained axially to 25 cm by the top of the electrolyte and by a scraper mounted to the vessel floor at the bottom. (The bottom scraper protrudes above the molten cadmium layer.) Uranium dendrites that are dislodged by the scrapers fall into the cadmium pool and dissolve. The uranium in the cadmium pool is recovered in a separate operation.

The power supply for the electrorefiner can be configured with the electrodes in a variety of ways depending on the desired operation. For introducing spent

[2] All compositions are listed in wt%.

Table 1
Spent fuel feedstock composition for one anode assembly (Batch ERBF04B)[a]

Active Metals, U, and Halogens	Mass (g)	Elements more noble than U	Mass (g)
Li	0.453	Al	0.156
Na	2.18×10^{2}	Si	33.3
Mg	1.89×10^{-2}	P	0.161
Cl	4.12	S	0.112
K	1.75	Ti	7.81
Br	0.673	V	0.33
Rb	9.74	Cr	4.26×10^{2}
Sr	23.6	Mn	62.8
Y	13.5	Fe	2.08×10^{3}
I	5.0	Co	0.554
Cs	81.9	Ni	4.86×10^{2}
Ba	32.5	Cu	0.437
La	29.5	Ge	4.54×10^{-2}
Ce	56.8	As	0.48
Pr	28.0	Se	2.01
Nd	96.1	Zr	1.12×10^{3}
Pm	2.67	Nb	0.16
Sm	16.9	Mo	1.32×10^{2}
Eu	1.11	Tc	18.9
Gd	0.408	Ru	42.4
Tb	1.75×10^{-2}	Rh	11.5
Dy	3.75×10^{-3}	Pd	9.22
Th	1.19×10^{-3}	Ag	0.459
U	8.28×10^{3}	Cd	0.718
Np	4.34	In	0.115
Pu	44.6	Sn	1.56
Am	1.00×10^{-3}	Sb	0.409
		Te	11.6
		Ta	0.151
		W	5.68×10^{-3}

[a]Elements with less than 10^{-3} g are not reported here. Column sorting is by atomic number.

fuel to the electrorefiner, the two power supply configurations are:

Direct Transport:
Anode: fuel dissolution baskets with chopped fuel segments,
Cathode: steel mandrel,

Anodic Dissolution:
Anode: fuel dissolution baskets with chopped fuel segments,
Cathode: cadmium pool.

The direct transport configuration is typical, with anodic dissolution performed at the tail end of a fuel batch. Only once (batch ERBF05A) has the anodic dissolution configuration been used to electrochemically dissolve the entire fuel batch.

The power supply for the electrorefiner was operated in the controlled current mode during direct transport. The desired current is input to the control software along with a cut-off voltage. After the current is turned on, the cell voltage rises with the increased resistance to uranium oxidation as the area of uranium decreases over time. The cell voltage is constantly compared to the cut-off voltage, and the power supply shuts down when the cell voltage exceeds the cut-off voltage. The current may then be reduced and the power supply restarted. Toward the end of an electrorefining experiment, the current and the throughput are low. Consequently, it is more expedient to remove the refined uranium deposit on the cathode and continue dissolving the spent fuel using the anodic dissolution configuration while harvesting the refined uranium deposit. The anodic dissolution configuration was operated in the controlled voltage mode.

During the electrorefining process, feedstock metals that are more active than uranium (e.g., sodium, cesium) accumulate in the molten salt electrolyte as their respective chlorides (discussed in Section 5.2). Noble metal fission products are ideally retained with the cladding hulls after the uranium is dissolved, as the desired flow sheet results in all of the noble metals being mixed with the cladding to produce the MWF. Noble metal fission products may also physically escape the cladding hulls as small particles to eventually dissolve in the cadmium pool or precipitate on a metal surface (e.g., the growing uranium deposit).

2.2. Destructive analyses

Three different sets of cladding hulls were examined straight out of the electrorefiner anode baskets. Each set

Table 2
Experimental conditions for electrochemical dissolution of irradiated fuel

Electrorefining batch	BF04B	BF05A
ER temperature (K)	723	723
Stock U in chopped segments (kg)	8.28	8.33
Equivalent U from fission products (kg)	1.43	1.40
Average anode voltage (V vs. Cd Pool)	0.19	0.44
Maximum anode voltage (V vs. Cd Pool)	0.38	0.60
Average current (A)	22	58
Anode RPM	25	25
Electrorefining mode	Direct transport, then anodic dissolution	Anodic dissolution
Cathode	Steel Mandrel, then cadmium pool	Cadmium pool

was run through the electrorefiner under different operating conditions. One set of cladding hulls was unirradiated, and the other two sets were irradiated. Since the LiCl/KCl eutectic salt adheres to the hulls upon removal from the electrorefiner, a water-wash was used to dissolve away the salt from the irradiated hulls. Water washing was conducted by placing a set of ten cladding hulls from each batch in a beaker of water and performing an ultrasonic cleaning procedure. The water-washing performed on the hulls from ERBF04B and ERBF05A was done to lower the activity of the hulls, thereby mitigating the negative effects (high levels of background, widened peaks) on the X-ray detector during subsequent SEM analysis. The chances of observing layers on the exposed surfaces of the cladding hull were also improved by removing the majority of the salt that may hide any fine features near the salt/cladding interface. For the unirradiated hulls, the adhering salt was distilled off by heating the salt-coated hulls in a vacuum induction furnace.

SEM analyses and optical metallography were performed on water-rinsed and distilled cladding hulls as follows: (1) each cladding hull was mounted to expose its respective cross-sections; (2) each mounted hull was then ground and polished through 1 μm diamond paste; (3) optical micrographs were taken of each polished, unetched sample (optical micrographs were subsequently taken of some etched samples after SEM analysis was completed); (4) each sample was then gold-coated to improve the conductivity of the sample; and (5) each sample was inserted into an ETEC Autoscan SEM fitted with a Kevex 8000 energy-dispersive spectrometer (EDS) from FISONS Instruments. SEM micrographs were taken and both semi-quantitative and quantitative analyses were performed.

Most of the irradiated samples that were analyzed had radiation fields between 500 and 750 mR/h (γ) at 2.5 cm. Some samples measured greater than 1.0 R/h (γ) at 2.5 cm, which made EDS analysis difficult. As mentioned earlier, high-activity samples impact the EDS detector by broadening the X-ray peaks, by increasing the levels of background, and by increasing the dead-time of the detector. In some cases, the activity of a sample was too high, and the detector was overwhelmed. Nevertheless, in all cases it was possible to take high-quality SEM micrographs of the cladding hull microstructures.

Chemical analyses were performed on ten cladding hulls from each batch of hulls to determine the amount of U and Zr that remained with each cladding hull. The ten cladding hulls were selected from the middle region of the anode dissolution baskets. The chemical analyses were performed by dissolving a large fraction of the individual cladding hull remains in a solution of HF and HNO_3. The dissolved uranium was extracted and analyzed by isotopic-dilution mass spectrometry (IDMS). The zirconium fraction was determined by inductively coupled plasma atomic emission spectroscopy (ICP-AES).

3. Initial condition of fuel elements discharged from EBR-II

The electrorefined, irradiated cladding hulls analyzed in this particular study had binary U–10Zr fuel and Type 316SS cladding. [3] They were irradiated, in EBR-II, to around 8.0 at.% burnup, where burnup is the amount of heavy atoms fissioned. Fig. 2 shows a representative optical micrograph of a transverse cross-section of a fuel element with U–10Zr fuel and Type D9 stainless steel cladding [4] irradiated to approximately 10 at.% burnup. The fuel elements irradiated to 8.0 at.% burnup would have analogous structures before being inserted into the electrorefiner.

A concentric three-zone fuel structure is typically observed in irradiated fuel elements with U–10Zr fuel and stainless steel cladding [6]. The original homogeneous U–10Zr alloy redistributes to form a Zr-rich region in the center of the fuel element, a Zr-depleted zone in the middle zone, and another Zr-enriched layer nearest the cladding. The driving force for this redistribution is a temperature gradient that exists from the center of a fuel element towards the radial periphery [6].

Near the fuel-cladding interface of a cross-sectioned fuel element, remnants of a Zr-rind can be observed. This is depicted in Fig. 3. The Zr-rind is formed during the initial injection casting of the U–10Zr alloy fuel. At localized areas of the fuel-cladding interface, interaction layers are observed where interdiffusion has occurred between fuel and cladding constituents. The fuel swells during irradiation, and at around 1.0 at.% burnup, the fuel contacts the cladding resulting in the observed interdiffusion [7]. A typical fuel-cladding interaction zone is presented in Fig. 4. The interaction zone consists of phases that contain U and Zr from the fuel, Fe, Ni, and Cr from the cladding, and various fission products (primarily lanthanides) that have diffused down a temperature gradient, during irradiation, to the fuel-cladding interface [8]. Other phases observed near the fuel-cladding interface include blocky particles that are composed mainly of noble metal fission products and two lanthanide-enriched phases. One of the lanthanide-enriched

[3] Type 316 stainless steel has the following nominal composition (in wt.%): 10–14Ni–16–18Cr–2Mn–2–3Mo–1Si–0.08C–0.03S–0.045P–bal.Fe.

[4] D9 stainless steel is a Ti-stabilized '316-like' stainless steel with lower Cr (14%) and higher Ni (16%) concentrations.

Fig. 2. Optical micrograph of the porous structure of a fuel element with U–10Zr fuel and D9 stainless steel cladding irradiated to approximately 10 at.% burnup in ERB-II. Note the thin layer of Zr-rind that appears between the fuel and the cladding.

phases contains Pd and the other does not [8]. These phases are shown in Fig. 5.

4. Results from analyses of cladding hulls after fuel dissolution in the electrorefiner

4.1. Chemical analyses

The results of the cladding hull chemical analyses for uranium and zirconium are presented in Table 3. Each sample for chemical analysis consisted of ten cladding hulls from the batches ERBF04B and ERBF05A. Chemical analyses were also conducted on the unirradiated cladding hulls, but no U or Zr was detected. From Table 3, it is clear that the cladding hulls from batch ERBF04B had relatively high levels of both U and Zr left behind after electrorefining, while ERBF05A had low levels of U and Zr. This difference is a consequence of the electrorefiner operating conditions for the two batches. Other components [e.g., cladding components (Fe, Ni, Cr, etc.) and noble metal fission products (Ru, Pd, etc.)] were also detected using chemical analysis but are not discussed here.

4.2. SEM/EDS analysis

4.2.1. Unirradiated cladding hulls

Fig. 6 shows a transverse cross-section of an unirradiated cladding hull taken from the electrorefiner. This

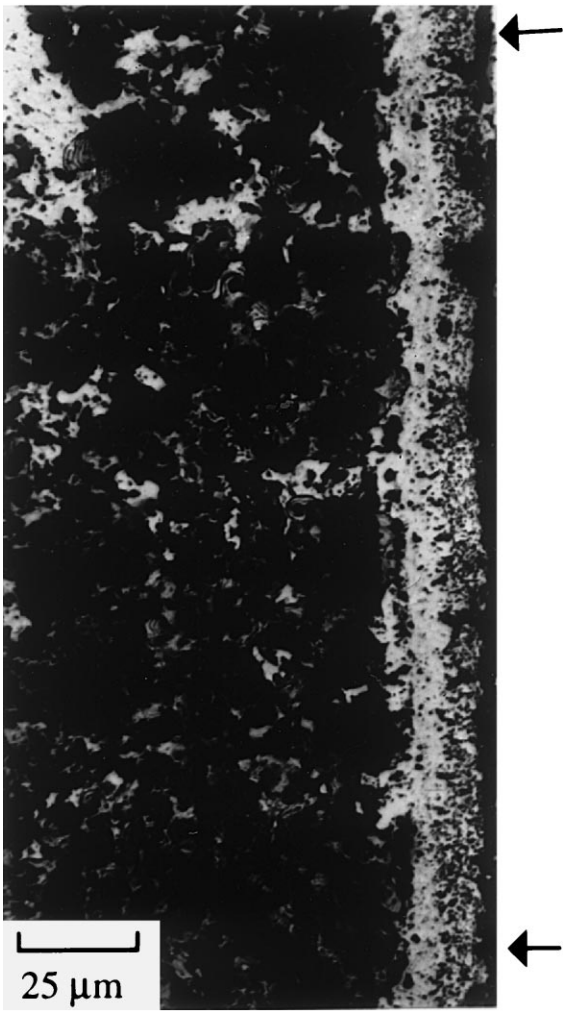

Fig. 3. An optical micrograph of the interface (identified with black arrows) between U–10Zr fuel and D9 stainless steel cladding in fuel element irradiated to approximately 10 at.% burnup in EBR-II. The fuel is to the left and the cladding is the bright region to the right. A gray Zr-rind layer appears between the fuel and the cladding.

cladding hull and the irradiated hulls discussed later are 375 μm thick. Only the original stainless steel components were detected in this sample using EDS analysis, and there was no evidence of any adhering material or unusual phases.

4.2.2. Irradiated cladding hulls

4.2.2.1. Cladding hulls from batch ERBF04B. Three cladding hulls from batch ERBF04B were analyzed using SEM/EDS. Fig. 7 is an SEM micrograph of a cladding hull sample from this batch. This sample had the least amount of adhering salt of the hulls analyzed from ERBF04B. Overall, the water-washing procedure

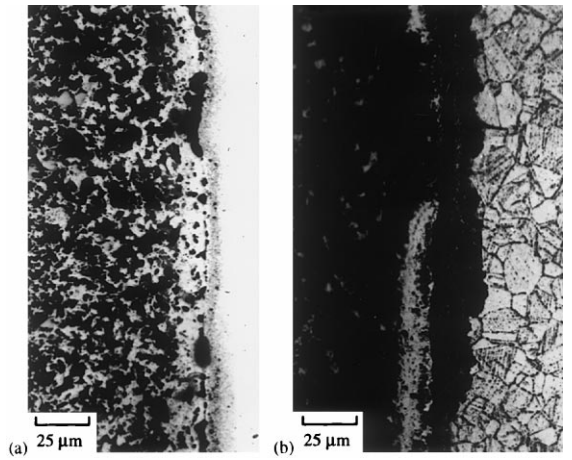

Fig. 4. Optical micrographs of the interface between U–10Zr fuel and D9 stainless steel cladding in a fuel element irradiated to approximately 10 at.% burnup in EBR-II. In (a) and (b) the fuel is to the left and the cladding is to right. (a) Shows the interaction layer in an unetched sample and (b) exhibits the interaction in a sample that was etched with oxalic acid. In (a) and (b) a Zr-rind layer is present between the cladding and the fuel.

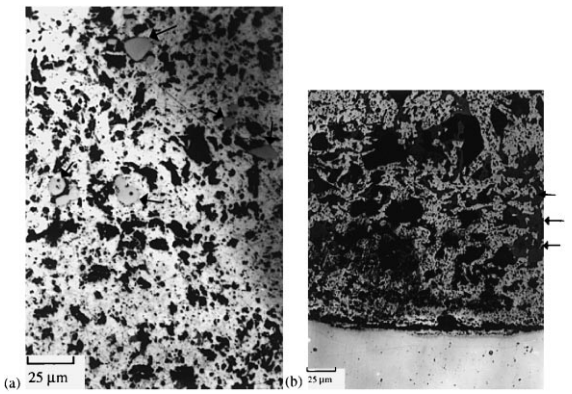

Fig. 5. Optical micrographs of: (a) 'blocky' noble metal-containing phases and (b) lanthanide-rich phases (both identified with black arrows) found in irradiated fuel near the fuel/cladding interface.

was incomplete. As would be expected, the cladding hull samples with the most salt left behind had the highest specific activities.

For the sample shown in Fig. 8, a minor adhering salt layer is observed, along with a Zr-rich layer (as confirmed by EDS analysis) which adheres to the cladding hull surface. The adhering Zr-rich layer contained a few percent of U and what appeared to be significant levels of Fe, Ni, and Cr. Due to the high activity of the samples analyzed in this investigation, an accurate

Table 3
Composition of U and Zr left with cladding hulls (wt%)

Batch	Av. U	Standard deviation for U	Av. Zr	Standard deviation for Zr
ERBF04B	11.0	1.3	18.3	2.8
ERBF05A	0.8	0.1	3.9	1.2

quantification of the phase compositions was not possible. It was only possible to identify the X-ray peaks that were present from the qualitative elemental analysis of these elements. The Zr-rich layer, along with the adhering salt, proved to be quite brittle, and, as a result, spalled easily away from the inner surface during handling and polishing of the cladding hull.

Another cladding hull from ERBF04B is illustrated in Fig. 9. This micrograph shows the continuous band of what appears to be the Zr-rind from the original fuel that remained after the electrorefining operation. In addition, the large amount of salt that adhered to this sample can be observed. Qualitative SEM/EDS analysis revealed the Zr-rind layer contained U, Fe, Ni, and Cr.

4.2.2.2. Cladding hulls from batch ERBF05A. A cross-sectioned ERBF05A cladding hull sample is presented in Fig. 10. Contrary to what was observed for the hulls from ERBF04B, the two hulls from ERBF05A that were analyzed were mostly free of any adhering salt. A minor amount of adhering salt can be observed attached to some regions of the interior surface of this cladding

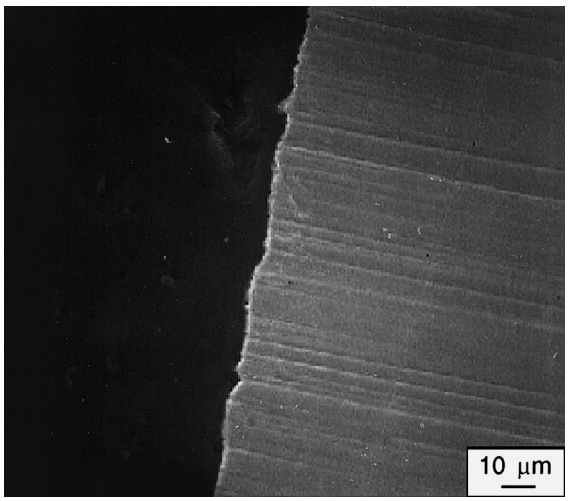

Fig. 6. SEM micrograph of the interior surface of an unirradiated cladding hull after electrorefining. Material to the left is mount and to right is Type 316SS cladding.

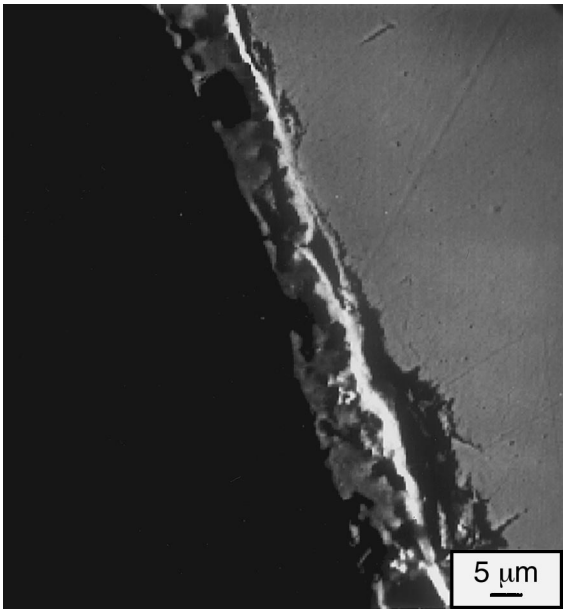

Fig. 7. SEM micrograph of the interior surface of a cladding hull from electrorefiner batch ERBF04B. From left to right, the black region is mount, the gray region is a LiCl/KCL salt layer, the bright\contrast region is a Zr-rich layer, and the medium-contrast region is cladding.

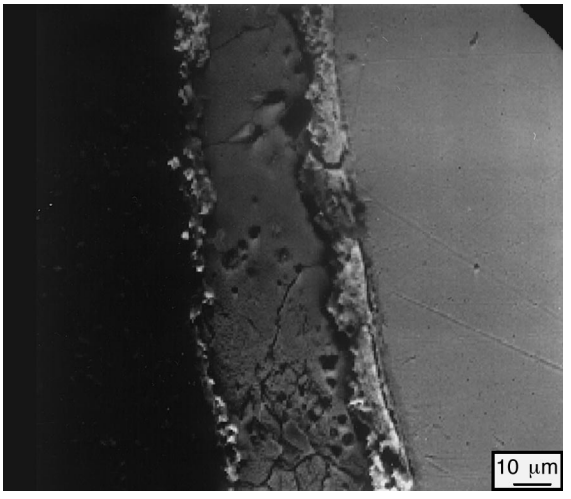

Fig. 8. SEM micrograph of the interior surface of a cladding hull from electrorefiner batch ERBF04B. From left to right, the black region is mount, the gray region is a LiCl/KCL salt layer, the bright-contrast region is a Zr-rich layer, and the medium-contrast region is cladding.

hull. In addition to the salt layer, a Zr-rich layer can be observed adjacent to the interior surface of the cladding hull.

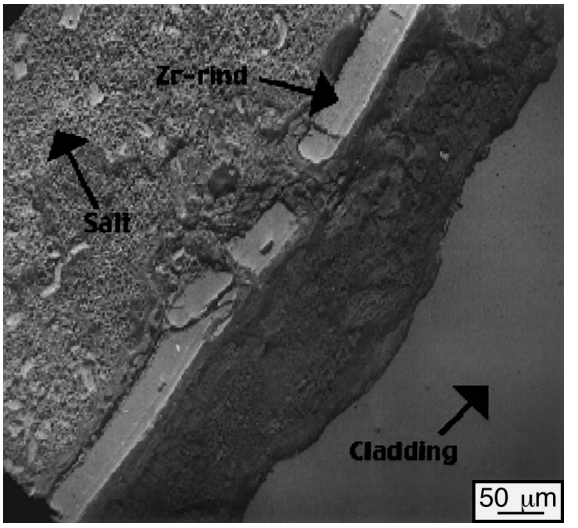

Fig. 9. SEM micrograph of the interior surface of a cladding hull from electrorefiner batch ERBF04B. To left is residual salt; the middle layer is Zr-rind; and to the right is cladding hull.

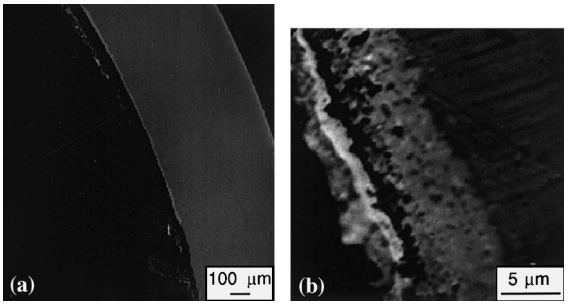

Fig. 10. SEM micrograph micrograph of the interior surface of an ERBF05A cladding hull. In (a) and (b) the material to the left is mount and to the right is cladding. In (b) the brightest-contrast layer is Zr-rich, and the medium-contrast material is salt.

5. Discussion

5.1. Material left behind with cladding hulls

The main features of the original, as-irradiated fuel elements, before electrorefining, are: (1) a three-zone fuel structure, where each zone has a different U and Zr composition; (2) 'blocky' particles, approximately 10 μm in diameter, that are present in the fuel and are enriched in noble metal fission products; (3) two types of lanthanide-rich phases, where one type of phase is enriched in Pd; (3) a zirconium rind on the radial periphery of the fuel slug that is a remnant of the original casting of the fuel and is present near the inner surface of the cladding;

and (4) interdiffusion zones that are present at localized areas of the inner surface of the cladding and contain primarily lanthanide fission products and cladding constituents.

After electrorefining, the components of the different phases found in the irradiated fuel are dissolved away in the electrorefiner and end up either in the LiCl/KCl eutectic salt, in the cadmium pool, with the U product that is deposited on the cathode, or with the cladding hulls. Even the interaction layers (described in Section 3) that are an intimate part of the cladding after irradiation to 8 at.% burnup, were dissolved during electrorefining. The interaction layers are concluded to be dissolved, because visually no layers are observed that look like ones observed in as-irradiated fuel elements, and no lanthanide fission products, which are major components of the interaction layers, were detected in the cladding hull sample chemical analysis.

The cladding hull interaction layers appear to have been present in these samples originally, before they were loaded into the electrorefiner. As shown in Fig. 11, the interior cladding hull surfaces are highly uneven. If no interaction ever occurred, then the inner surface of the cladding hulls would have remained smooth, like they were when the fuel elements were initially cast. However, since the surfaces were uneven, some interaction must have occurred, and the interaction previously observed for irradiated fuel is considered the cause [7,8]. Only the portion of the cladding hull that was unreacted was left behind.

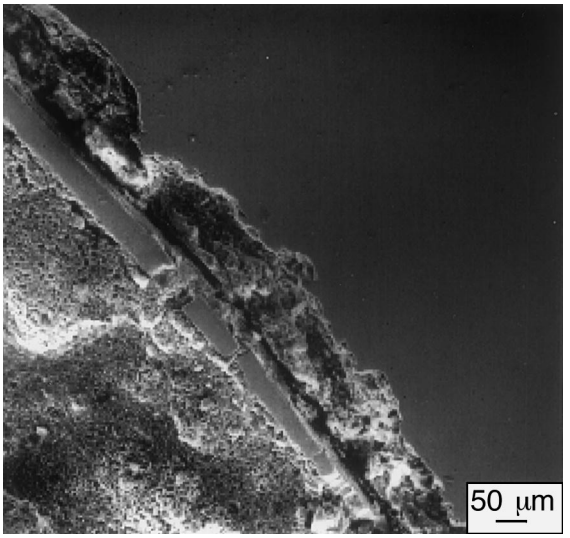

Fig. 11. SEM micrograph showing the uneven interior surface of an ERBF04B cladding hull. Salt is present to left; cladding is to the right; and a Zr-rind layer is in middle.

Of the material that remains with the cladding hulls after electrorefining, a significant fraction of it is intimately adhering to the interior and exterior surfaces of the cladding hulls. Based on the results of chemical and SEM analyses of the ERBF04B and ERBF05A cladding hulls, this adhering material mainly consists of Zr-rich layers that contain U and small amounts of the major stainless steel components. Chemical analysis has shown that noble metal constituents are present in very low levels with the cladding hull samples. Based on the morphology of the layers, they appear to have been electrodeposited, up to a thickness of around 5.0 μm (see Fig. 7), onto the cladding hulls. The layers are very uniform and do not appear as localized clumps of material, which may have suggested some other mechanism by which the Zr and U could have been left behind with the cladding hulls (e.g., incomplete dissolution of the fuel may have left clumps of material).

In some isolated cases, some of the alloy fuel has been left behind with cladding hulls in the form of 'islands' of material (these samples are not discussed in this paper), but even in these circumstances layers appear on the interior and exterior surfaces of the cladding hulls. The 'islands' of the original fuel would result from incomplete dissolution of the fuel, whereas the uniform layers are evidence of electrodeposition.

For some cladding hulls, other layers enriched in zirconium are observed that are not deposited, and they did not directly adhere to any cladding hull surfaces. These layers appear to be undissolved Zr-rind and residues from the original fuel. This rind not only contains Zr, but it also contains minor amounts of stainless steel components of Fe, Ni, and Cr, along with some U. The non-Zr components are most likely a result of the interdiffusion processes that occurred during irradiation of the fuel elements. As mentioned earlier, the fuel, which swells during irradiation, contacts the cladding, and interdiffusion between fuel and cladding constituents is initiated. Since the Zr-rind is found at the outer periphery of the fuel, the Zr-rind is the portion of the fuel to come into contact with the cladding first. Then, the constituents of the fuel alloy, rind, and cladding interdiffuse, resulting in the presence of U, Fe, Ni, and Cr in the Zr-rind [9].

In terms of relating the percentages of U and Zr left behind with the cladding hulls to the morphology of the residual material, the cladding hulls with the highest levels of remaining U and Zr can be correlated to higher levels of remaining Zr-rind. This is in addition to the Zr-rich layers that are deposited on the exposed surfaces of the cladding hulls. In the case where 99.2% of the U and 96.1% Zr are dissolved from the cladding hull, no Zr-rind is observed and the residual Zr and U are contained in the uniform, deposited Zr-rich layers.

5.2. Mechanism for uranium metal to be deposited on exterior surfaces of cladding

The observed layers of Zr and U depositing on the exterior cladding hull surfaces after electrorefining are explainable. As indicated in Table 1, some metals present are more active than uranium metal. These include the thermal bond sodium, alkali, alkali earths, and lanthanide metals. These metals will react to displace UCl_3 in the electrolyte, e.g.,

$$3Na + UCl_3 \rightarrow 3NaCl + U \tag{3}$$

or in general,

$$xM + yUCl_3 \rightarrow xMCl_y + yU. \tag{4}$$

The uranium metal that is produced from the above reactions may deposit on the cladding exterior or on the spent fuel itself. When the U^{3+} in the electrolyte contacts the exterior surface of the cladding, uranium metal will deposit on the exterior surface and active metals will oxidize from the exposed fuel surface. An electronic current will flow through the steel of the cladding (Fig. 12) to support the oxidation–reduction reaction. This reaction mechanism is similar to that for short-circuiting a battery. On the other hand, U^{3+} in the electrolyte can come into contact with the active metals on the exposed fuel and chemically react. Uranium could then deposit on the exposed fuel while the active metals are dissolved via the chemical reaction. However, the exterior surfaces of the cladding represent twice the surface area of the exposed fuel, so that reaction on the exterior surfaces can predominate.

Because of the above mechanism, the amount of charge (number of coulombs) necessary to oxidize the uranium in the anode assembly will be greater than the charge corresponding to the stock amount of uranium in the spent fuel alone. With Faraday's Law, the amount of charge theoretically required to oxidize the stock amount of uranium in the anode assembly may be calculated (8.3 kg in Table 1, or 9.97×10^6 coulombs). This value can be compared to the charge actually required to nearly exhaust the uranium from the baskets, (approximately 11.5×10^6 coulombs). The difference (1.55×10^6 coulombs) between the actual charge and the theoretical charge for stock uranium agrees well with the additional amount of charge expected for the uranium reduced by the active metals (1.83×10^6 coulombs for approximately 1.5 kg U). Moreover, approximately 300 g of uranium is typically retained in the hulls (in the effort to retain noble metals). Allowing for the 300 g of uranium to be retained in the hulls, the actual charge almost exactly agrees with the charge for the amount of uranium anodically dissolved (stock uranium plus uranium from reaction less 300 g).

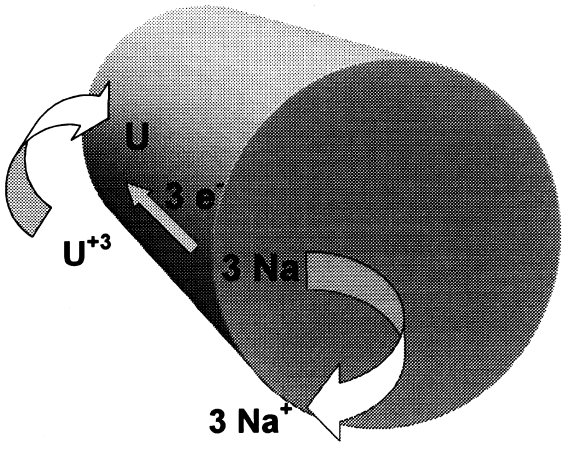

Fig. 12. Schematic diagram depicting the electronic current flow through the stainless steel cladding to support the oxidation–reduction reaction.

5.3. Mechanism for zirconium metal to be deposited on exterior surfaces of cladding

When anode voltage is large enough, the oxidation of zirconium from the fuel matrix occurs. Thus the reactions

$$Zr \rightarrow Zr^{2+} + 2e-, \tag{5}$$

and

$$Zr \rightarrow Zr^{4+} + 4e- \tag{6}$$

can represent a fraction of the current at the anode, in addition to the uranium oxidation reaction. The threshold for oxidation of zirconium at the anode can be approximated by taking the difference of the standard reduction potentials in an electromotive force series [10], which is approximately 0.4 V. (The difference in standard reduction potentials is an approximation in that all species involved are not present in the electrorefiner at unit activity.) Once zirconium ions (e.g., Zr^{+2}) are dissolved in the molten salt electrolyte, zirconium can later deposit onto the exterior surface of the cladding, by exactly the same mechanism that uranium deposits onto the exterior surface of the cladding.

Even while current is impressed on the electrorefiner cell, uranium is a more active metal than zirconium. If the anode voltage is marginally at the zirconium oxidation threshold or drops below it, Zr^{+2} ions in contact with uranium or cladding can be displaced by uranium metal in an oxidation–reduction reaction:

$$3Zr^{+2} + 2U \rightarrow 3Zr + 2U^{+3}. \tag{7}$$

Here, as in the mechanism for uranium deposition on the exterior cladding surface, the cladding provides the short-circuit for the electrons in the oxidation–reduction reaction, i.e.,

$$3Zr^{2+} + e- \rightarrow 3Zr \quad (8)$$

and

$$2U \rightarrow 6e - +2U^{+3}. \quad (9)$$

However, uranium is the more active metal and is oxidized while the more noble metal zirconium is deposited on the cladding surface. The thermodynamic driving force for this reaction is even greater if some Zr^{2+} is present at the cladding surface when the current to the cell is turned off and the anode voltage decays to zero. For the reaction to occur when the current is turned off, some residual uranium must be present with the hulls, which has been on the order of 300 g uranium.

When results for the unirradiated cladding hulls are compared with the results for the irradiated cladding hulls, the unirradiated cladding hulls, which contained simulated fuel, showed no signs of uranium or zirconium layers on the interior or exterior surfaces. This difference can be explained by the complete dissolution of the simulated fuel from the unirradiated cladding hulls. The simulated fuel may have in fact dissolved more readily since there was no metal redistribution and alloy formation in the absence of irradiation. The observed cell resistances support this explanation.

The highest cell resistance observed for the unirradiated, simulated fuel was 16.8 Ω, which occurred for the complete dissolution of uranium and zirconium. On the other hand, the highest cell resistance observed for the irradiated fuel Batch ERBF04B was 21.0 Ω. [5] Note this maximum cell resistance occurred for incomplete uranium dissolution. Furthermore, virtually all irradiated fuel batches electrorefined under direct transport required a cell resistance 30% greater than the unirradiated batches in order to oxidize most or all the uranium. These observations urge the conclusion that metal redistribution and alloy formation restrict uranium dissolution by lowering the mass transfer coefficient or the activity of uranium metal (e.g., the fuel matrix restricts the access of the uranium surface for electrochemical oxidation, [11,12]). Hence a higher cell resistance is needed for a comparable extent of uranium dissolution in the irradiated fuel relative to the unirradiated fuel.

[5] The cell resistance for Batch ERBF05A cannot be included in the comparison, since uranium was anodically dissolved to the cadmium pool. This method for uranium oxidation always yields a lower resistance, since the distance between the fuel dissolution baskets and the cadmium pool is considerably less than the distance between the fuel dissolution baskets and the cathode mandrel.

6. Conclusions

The following conclusions can be drawn from the SEM analyses: (1) Zr-rich layers, with a few percent uranium, are deposited on the exposed surfaces of the irradiated cladding hulls in the electrorefiner; (2) Zr-rich layers appear on cladding hulls even when most of the fuel has been dissolved away, i.e. 99.2% of the U and 96.1% of the Zr; (3) where detectable fuel is left behind in the cladding hulls, the majority of the remaining material consists of the Zr-rind , which was formed during the injection casting of the original fuel; and, (4) no evidence of the fuel-cladding interaction layers, which is present in U–10Zr irradiated to 8 at.% burnup, was found on the interior surface of the cladding hulls.

Acknowledgements

The US Dept. of Energy supported this work under contract W-31-109-Eng-38. Argonne National Laboratory is operated by the University of Chicago. Acknowledgment is given to A.B. Cohen of the Alpha Gamma Hot Cell Facility for his assistance in conducting the SEM analyses of the irradiated cladding hulls and to the Analytical Laboratory personnel at ANL-West who performed the water-washing and chemical analyses of the cladding hull samples.

References

[1] J.P. Ackerman, T.R. Johnson, L.S.H. Chow, E.L. Carls, W.H. Hannum, J.J. Laidler, Prog. Nucl. Energy 31 (1997) 141.

[2] D.D. Keiser, Jr., B.R. Westphal, Proc. of the DOE Spent Nuclear Fuel and Fissile Materials Management Conference, Charleston, SC, 8–11 September 1998, ANS, La Grange Park, IL, 1998, submitted.

[3] S.M. McDeavitt, D.P. Abraham, D.D. Keiser, Jr., J.Y. Park, Proceedings Second International Symposium on Extraction and Processing for the Treatment and Minimization of Wastes, in: V. Ramachandran, C.C. Nesbitt (Eds.), Scottsdale, AZ, 27–30 October 1996, Minerals, Metals, & Materials Society, Warrendale, Pennsylvania, 1996, p. 177.

[4] R.D. McKnight, J.A. Stillman, B.J. Toppel, and H.S. Khalil, Proceedings Topical Meeting on Advances in Reactor Physics, vol. 1, Knoxville, TN, 11–15 April 1994, ANS, La Grange Park, IL, 1994, p. 150.

[5] R.D. McKnight, Proceedings Topical Meeting on Advances in Reactor Physics, vol. 2, Charleston, SC, 8–11 March 1992, ANS, La Grange Park, IL, 1992, p. 69.
[6] G.L. Hofman, S.L. Hayes, M.C. Petri, J. Nucl. Mater. 227 (1996) 277.
[7] G.L. Hofman, L.C. Walters, T.H. Bauer, Prog. Nucl. Energy 31 (1997) 83.
[8] G.L. Hofman, in: R.W. Cahn, P. Haasen, E.J. Kramer (Eds.), Materials Science and Technology: A Comprehensive Treatment, vol. 10, VCH, New York, 1994, p. 1.
[9] D.D. Keiser, Jr., A.B. Cohen, to be published.
[10] J.A. Plambeck, in: A.J. Bard (Ed.), Encyclopedia of Electrochemistry of the Elements, vol. X, Fused Salts, Marcel Dekker, New York, 1976, p. 68.
[11] A.J. Bard, L.R. Faulkner, Electrochemical Methods, Wiley, New York, 1980, p. 27.
[12] J.O'M. Bockris, A.K.N. Reddy, Modern Electrochemistry, vol. 2, Plenum Rosetta, New York, 1973, p. 1223.